

Thermalization, Isotropization and Elliptic Flow from Nonequilibrium Initial Conditions with a Saturation Scale

M. Ruggieri,¹ F. Scardina,^{1,2} S. Plumari,^{1,2} and V. Greco^{1,2}

¹*Department of Physics and Astronomy, University of Catania, Via S. Sofia 64, I-95125 Catania*

²*INFN-Laboratori Nazionali del Sud, Via S. Sofia 62, I-95123 Catania, Italy*

In this article we report on our results about the computation of the elliptic flow of the quark-gluon-plasma produced in relativistic heavy ion collisions, simulating the expansion of the fireball by solving the relativistic Boltzmann equation for the parton distribution function tuned at a fixed shear viscosity to entropy density ratio η/s . Our main goal is to put emphasis on the role of a saturation scale in the initial gluon spectrum, which makes the initial distribution far from a thermalized one. We find that the presence of the saturation scale reduces the efficiency in building-up the elliptic flow, even if the thermalization process is quite fast $\tau_{therm} \approx 0.8$ fm/c and the pressure isotropization even faster $\tau_{isotr} \approx 0.5$ fm/c. The impact of the non-equilibrium implied by the saturation scale manifests for non-central collisions and can modify the estimate of the viscosity respect to the assumption of full thermalization in p_T -space. We find that the estimate of η/s is modified from $\eta/s \approx 2/4\pi$ to $\eta/s \approx 1/4\pi$ at RHIC and from $\eta/s \approx 3/4\pi$ to $\eta/s \approx 2/4\pi$ at LHC. We complete our investigation by a study of the thermalization and isotropization times of the fireball for different initial conditions and values of η/s showing how the latter affects both isotropization and thermalization. Lastly, we have seen that the range of values explored by the phase-space distribution function f is such that at $p_T < 0.5$ GeV the inner part of the fireball stays with occupation number significantly larger than unity despite the fast longitudinal expansion, which might suggest the possibility of the formation of a transient Bose-Einstein Condensate.

PACS numbers: 12.38.Aw, 12.38.Mh

Keywords: Heavy ion collisions, Color Glass Condensate, Shear Viscosity, Elliptic Flow, Transport Theory.

I. INTRODUCTION

In the last decade it has been reached a general consensus that Ultra-relativistic heavy-ion collisions (uRHICs) at the Relativistic Heavy-Ion Collider (RHIC) and the Large Hadron Collider (LHC) create a hot and dense strongly interacting quark and gluon plasma (QGP) [1–4]. A main discovery has been that the QGP has a very small shear viscosity to density entropy, η/s , which is more than one order of magnitude smaller than the one of water [5, 6], and close to the lower bound of $1/4\pi$ conjectured for systems at infinite strong coupling [7]. A key observable to reach such a conclusion is the elliptic flow [9],

$$v_2 = \langle \cos(2\varphi_p) \rangle = \left\langle \frac{p_x^2 - p_y^2}{p_x^2 + p_y^2} \right\rangle, \quad (1)$$

with φ_p being the azimuthal angle in the transverse plane and the average meant over the particle distribution. In fact, the expansion of the created matter generates a large anisotropy of the emitted particles that can be primarily measured by v_2 . An hadronic system would generate a v_2 about a factor 2-3 smaller than the measured one [8] and this is one of the hints that the system created at RHIC and LHC is of non-hadronic nature.

The origin of v_2 is the initial spatial eccentricity,

$$\epsilon_x = \frac{\langle y^2 - x^2 \rangle}{\langle x^2 + y^2 \rangle}, \quad (2)$$

of the overlap region in non-central collisions, which is responsible for different pressure gradients in the trans-

verse plane thus favoring flow preferably along the x direction rather than y direction. The observed large v_2 is considered a signal of a very small η/s because it means that the system is very efficient in converting ϵ_x into an anisotropy in the momentum space v_2 , a mechanism that would be strongly damped in a system highly viscous that dissipates and smooths anisotropies [10–12]. Quantitatively both viscous hydrodynamics [10, 11, 13–15], and transport Boltzmann-like approaches [16–21] agree in indicating an average η/s of the QGP lying in the range $4\pi\eta/s \sim 1 - 3$.

Along with the existence of a deconfined QGP matter and the understanding of its properties, the uRHIC program offers the opportunity to verify the picture in which at very high energy the two colliding nuclei are described as two sheets of Color Glass Condensate (CGC) [22–24], see [25–28] for reviews. The CGC in the nuclei would be primarily generated by the very high density of the gluon distribution function at low x (parton momentum fraction), which triggers a saturation of the distribution for p_T below a saturation scale, Q_s . The determination of the shear viscosity η/s of the QGP and the search for the CGC are related. In fact, the main source of uncertainty for η/s comes from the unknown initial conditions of the created matter [13, 30–32] that imply quite different eccentricities ϵ_x .

A simple geometrical description through the Glauber model [33] predicts a ϵ_x smaller at least 25-30% than the eccentricity of the CGC, for most of the centralities of the collisions, see for example results within the Kharzeev-Levin-Nardi (KLN) model [34, 35, 50], factorized KLN (fKLN) model [36], Monte Carlo KLN (MC-KLN) model

[36, 37] and dipole model [38, 50]. In fact, the saturation of gluon distribution function is stronger in the central overlapping region, making the space distribution sharper than the one coming from a simple geometrical overlap. Other CGC models like the ones based on the solution of the classic Yang-Mills (CYM) equations predict a somewhat smaller initial eccentricity [39]. However the effect we discuss in the present paper is mainly related to the saturation effect in momentum space and not in the r -space that determines the eccentricity, even if certainly to consider CYM initial conditions is an important task considering the success it has in predicting the collective flow anisotropies $v_n = \langle \cos(n\phi) \rangle$ with $n \geq 2$ [51].

In this article, we report our results about the computation of the elliptic flow of the quark-gluon-plasma produced in relativistic heavy ion collisions, simulating the expansion of the fireball by solving the relativistic Boltzmann equation for the parton distribution function tuned at a fixed shear viscosity to entropy density ratio η/s [19, 20, 43, 44]. In this context the advantage of using kinetic theory is that starting from a one-body phase space distribution function $f(x, p)$, and not from the energy-momentum tensor $T^{\mu\nu}$, it is straightforward to initialize simulations from a non-equilibrium distribution function, like the one characterizing the KLN model, while the hydrodynamics relies on the gradient expansion of the stress tensor and therefore is applicable only if initial deviations from local equilibrium are small. It is worth noticing that kinetic theory has also attracted interest as a tool to derive equations for the hydrodynamical evolution of a fluid starting from a microscopic theory [84, 85].

In this study we assume that the initial condition in configuration and momentum space arising from the melting of the CGC is given by the KLN model. In fact the KLN initial condition that has been largely employed to study the dynamics of HIC and the viscosity of the QGP [13, 30, 31, 37, 58–60]. The uncertainty in the initial condition translates into an uncertainty on η/s of at least a factor of two as estimated by mean of several viscous hydrodynamical approaches [13, 30–32]. More explicitly, the experimental data of $v_2(p_T)$ at the highest RHIC energy are in agreement with a fluid with $4\pi\eta/s \approx 1$ according to viscous hydrodynamics simulation, assuming a standard Glauber initial condition. Assuming an initial fKLN or MC-KLN space distribution the comparison favors a fluid at $4\pi\eta/s \approx 2$. The reason is the larger initial ϵ_x of the fKLN, which leads to larger v_2 unless a large η/s is considered. We point out that the implementation of the shattered CGC initialization in hydrodynamics takes into account only the different space distribution respect to a geometric Glauber model, discarding the key and more peculiar feature of the damping of the distribution for p_T below the Q_s saturation scale. We have found by mean of kinetic theory that this has a significant impact on the build-up of v_2 .

In order to frame our work correctly, we refer to the

standard picture of the evolution of the fireball produced in the heavy ion collision, so we can identify the moment in which our approach is valid. The commonly accepted picture goes as follows: at $\tau = 0^-$ the two high energy colliding nuclei are described as two thin sheets of color-glass condensate, which after the collision turns at $\tau = 0^+$ into an out-of-equilibrium glasma state, which consists of a background of chromomagnetic and chromoelectric flux tubes, on the top of which quantum fluctuations are produced and cause the decay of the glasma itself to a parton liquid as the system expands. This parton system then equilibrates and the evolution is governed by viscous hydro. During the very early evolution of the glasma, the initial negative longitudinal pressure becomes positive because of the breaking of the color strings, see for example [52–54]. The decay causes the fields become very weak within a fraction of fm/c: we denote this time by τ_0 . From this time a description of the system as a pure interacting partons liquid becomes reliable, and can be described by kinetic theory. We therefore start our simulations from τ_0 . We assume $\tau_0 \sim Q_s^{-1} = 0.2$ fm/c in this work; however we have checked that our main results on the elliptic flow are not affected significantly by shifting the initial time to reasonably larger times. Within our framework the longitudinal pressure P_L at $\tau = \tau_0$ is positive, in agreement with recent calculations within Classic-Yang Mills statistical approach [53] or within kinetic theory at fixed η/s with a gauge field in abelian dominance [52]. Our main purpose in this study is to take into account strong deviations from local equilibrium in the initial condition, which naturally arise when the KLN model is used in the calculations: these kind of deviations are not affordably treated within viscous hydrodynamics even if in principle non vanishing bulk and shear energy tensor at τ_0 may account for it. Anyway, we will show that our description reproduces the hydrodynamics results when a proper thermalized initial condition is prepared in our simulations.

The plan of the article is as follows. In Section II, we review the initial conditions we use in the simulations, namely the factorized glasma the Glauber initial conditions. In Section III, we review our approach to kinetic theory at fixed η/s . In Section IV, we present our results on thermalization and isotropization of the fireball, as well as on the time evolution of the parton distribution function in the expanding system. In Section V, we present and discuss our results on the elliptic flow. Finally in Section VI, we draw our conclusions.

II. GLUON PRODUCTION IN THE KLN APPROACH

In order to prepare the initial condition in coordinate and momentum space of a melted glasma state we adopt the model which was firstly introduced by Kharzeev, Levin and Nardi [34] (KLN model), with particular ref-

erence to the factorized-KLN (fKLN) approach as introduced in [36, 37], in which the coordinate space distribution function of gluons arising from the melted glasma is assumed to be

$$\frac{dN_g}{dyd^2\mathbf{x}_\perp} = \int d^2\mathbf{p}_T p_A(\mathbf{x}_\perp)p_B(\mathbf{x}_\perp)\frac{dN}{d\mathcal{P}}, \quad (3)$$

where $dN/d\mathcal{P}$ corresponds to the momentum space distribution in the k_T factorization hypothesis [40, 41],

$$\begin{aligned} \frac{dN}{d\mathcal{P}} &= \frac{4\pi^2 N_c}{N_c^2 - 1} \frac{1}{p_T^2} \int^{p_T} d^2\mathbf{k}_T \alpha_S(Q^2) \\ &\times \phi_A(x_1, k_T^2; \mathbf{x}_\perp) \\ &\times \phi_B(x_2, (\mathbf{p}_T - \mathbf{k}_T)^2; \mathbf{x}_\perp), \end{aligned} \quad (4)$$

and $d\mathcal{P} = dyd^2\mathbf{x}_T d^2\mathbf{p}_T$. Here $x_{1,2} = p_T \exp(\pm y)/\sqrt{s}$ correspond to the longitudinal momentum fraction carried by the gluons belonging to the two colliding nuclei which produce a gluon with transverse momentum p_T and rapidity y ; the ultraviolet cutoff in the k_T integral in Eq. (3) is $p_T = 3$ GeV/ c for the case of Au-Au collisions at $\sqrt{s} = 200A$ GeV, while we take $p_T = 4$ GeV/ c for the case of Pb-Pb collisions at $\sqrt{s} = 2.76A$ TeV; α_S denotes the strong coupling constant, which is computed at the scale $Q^2 = \max(k_T^2, (\mathbf{p}_T - \mathbf{k}_T)^2)$ according to the one-loop β function but frozen at $\alpha_s = 0.5$ in the infrared region as in [35, 38, 42]. In Eq. (3) $p_{A,B}$ denote the probability to find one nucleon at a given transverse coordinate, namely

$$p_A(\mathbf{x}_\perp) = 1 - (1 - \sigma_{in} T_A(\mathbf{x}_\perp)/A)^A, \quad (5)$$

where σ_{in} is the inelastic cross section and T_A corresponds to the usual thickness function of the Glauber model.

Equation (3) is based on the factorization hypothesis, which is known to work fairly in the case of proton-proton as well as proton-nucleus collisions but it is violated in the case of a nucleus-nucleus collision [55]. However, we do not aim at considering the exact spectrum of a glasma, that may be computed for example within the CYM approach [55, 56]; rather we wish to study another issue, that is how the initial nonequilibrium distribution in momentum space, in particular one with a saturation scale built in, affects the building up of the elliptic flow. Furthermore, the KLN initial condition is still largely employed in hydrodynamics simulations to test the impact of initial conditions on different observables [58–67]. For simplicity, and also to uniform our language to that commonly adopted in hydro simulations, we still refer to the initial condition specified by Eq. (3) as to the melted-glasma initial condition.

The main ingredient to specify in Eq. (4) is the unintegrated gluon distribution function (uGDF) for partons coming from nucleus A , which is assumed to be:

$$\phi_A(x_1, k_T^2; \mathbf{x}_\perp) = \frac{\kappa Q_s^2}{\alpha_s(Q_s^2)} \left[\frac{\theta(Q_s - k_T)}{Q_s^2 + \Lambda^2} + \frac{\theta(k_T - Q_s)}{k_T^2 + \Lambda^2} \right], \quad (6)$$

which embeds saturation of the distribution for $p_T < Q_s$; a similar equation holds for partons belonging to nucleus B . Following [36] we take the saturation scale for the nucleus A as

$$Q_{s,A}^2(x, \mathbf{x}_\perp) = Q_0^2 \left(\frac{T_A(\mathbf{x}_\perp)}{1.53p_A(\mathbf{x}_\perp)} \right) \left(\frac{0.01}{x} \right)^\lambda, \quad (7)$$

with $\lambda = 0.28$, and similarly nucleus B . The scale Q_0 regulates the average value of the saturation scale on the transverse plane. Equation (7) implies that for a fixed value of x , the larger the nucleon density the larger the saturation scale, since $Q_s^2 \propto T_A$ for large T_A ; however in the limit $T_A \rightarrow 0$, which is realized in the peripheral region of each of the two colliding nuclei, Equation (7) implies that Q_s does not vanish as T_A . In fact if $T_A \rightarrow 0$ then from Eq. (5) we get $T_A/p_A \rightarrow 1/\sigma_{in}$, which implies that Q_s is nonzero in this limit, and coincides with the saturation scale of a nucleon [36].

For our simulations of Au-Au collisions at RHIC energy we take $Q_0^2 = 1$ GeV², which gives $\langle Q_s \rangle \approx 1$ GeV in the case $b = 0$, at $y = 0$, $\sqrt{s} = 200A$ GeV and $x = 0.01$, where the average is understood in the transverse plane. This numerical value is smaller than the one commonly used in hydrodynamic simulations, where $\langle Q_s \rangle \approx 1.4$ GeV, see for example [13, 36, 37], and that we used in our previous work [21]. We prefer to use a smaller value of the average saturation scale in our simulations because in this way we can shift from the fKLN initial condition to the other ones obtaining the same final spectra, without the need to tweak the kinetic freezeout parameters when changing among the several initial conditions. In this way, the differences between the various systems we study here are confined in the initial configuration, while the dynamics of the freezeout is not affected by the initial conditions. However, to show the impact of the saturation scale we will discuss both the cases $Q_0 = 1$ GeV and $Q_0 = 2$ GeV in agreement with the estimates of [57], for the Pb-Pb collisions simulations at the LHC energy.

In Fig. 1 which we plot the averaged value of Q_s on the transverse plane,

$$\langle Q_s \rangle = \frac{\int d^2\mathbf{x}_T Q_s dN/d\mathcal{P}}{\int d^2\mathbf{x}_T dN/d\mathcal{P}}, \quad (8)$$

with Q_s given by Eq. (7) and the weight function by Eq. (4), for the cases of a Au-Au collision at $\sqrt{s} = 200A$ GeV and a Pb-Pb collision at $\sqrt{s} = 2.76A$ TeV, for gluons at $y = 0$ and $p_T = 2$ GeV, corresponding to $x = 0.01$ in the case of the Au-Au collision and to $x = 7 \times 10^{-4}$ in the case of the Pb-Pb collision.

III. KINETIC THEORY AT FIXED η/s

In our study we employ transport theory as a base of a simulation code of the fireball expansion created in relativistic heavy-ion collision [19, 20, 43, 44], therefore the gluon distribution function $f_1(\mathbf{x}, \mathbf{p}, t)$ evolves according

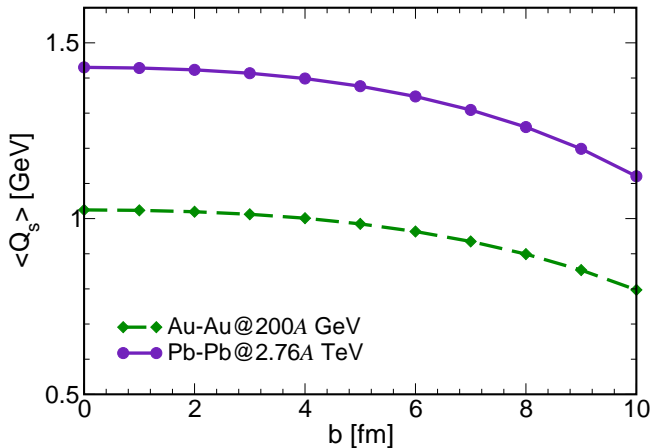


FIG. 1: (Color online) Saturation scale Q_s averaged over the transverse plane for the cases of a Au-Au collision at $\sqrt{s} = 200A$ GeV (green dashed line) and a Pb-Pb collision at $\sqrt{s} = 2.76A$ TeV (solid indigo line). All the calculations correspond to gluons produced at $y = 0$ and $p_T = 2$ GeV, and $Q_0 = 1$ GeV.

to the Relativistic Boltzmann Transport (RBT) equation:

$$p_\mu \partial^\mu f_1 = C[f], \quad (9)$$

where $C[f]$ is the collision integral,

$$C[f] = \int d\Gamma_2 d\Gamma_{1'} d\Gamma_{2'} (f_{1'} f_{2'} - f_1 f_2) \times |\mathcal{M}|^2 \delta^4(p_1 + p_2 - p_{1'} - p_{2'}), \quad (10)$$

with $d^3\mathbf{p}_k = 2E_k(2\pi)^3 d\Gamma_k$, and \mathcal{M} corresponds to the transition amplitude.

At variance with the standard use of transport theory, in which one fixes a set of microscopic processes whose scattering matrix is fed into the collision integral, we have developed an approach that, instead of focusing on specific microscopic calculations or modelings for the scattering matrix, fixes the total cross section in order to have the wanted η/s . By means of this procedure we are able to use the Boltzmann equation to simulate the dynamical evolution of a fluid with specified shear viscosity, in analogy to what is done within hydrodynamical simulations. The advantage of the kinetic theory approach at fixed η/s , compared to hydro simulations, is twofold: firstly starting from $f(x, p)$, and not from $T^{\mu\nu}$, it is direct to incorporate non-equilibrium initial conditions. Secondly we do not need to specify an ansatz for the deviations δf from equilibrium due to viscous corrections. This approach to kinetic theory has been also considered in [74, 75] where it has been shown that transport theory at fixed η/s reproduces the results of viscous hydrodynamics for one-body observable like $T^{\mu\nu}$ or entropy density also in the limit in which the system is not in the dilute regime. This is not surprising because

looking at the Boltzmann collision integral in terms of viscosity allows the analytical derivation of second order viscous hydrodynamics [78, 79].

In this article we consider only the $2 \leftrightarrow 2$ processes to compute the collision integral. One may think that the introduction of the higher order processes would result naturally in a change of the available phase space of partons, but once the system is close to an hydro regime where many collisions happens in a very short time respect to the expansion time scale and system size, the detail of the single scattering is lost and what matters is the viscosity of the fluid. Of course one can expect that the microscopic details of the scattering arises at large p_T where a hydro-like description in terms of a gradient expansion of the stress tensor breaks down; in the regime of small and moderate p_T , which is the one we are interested to in this study, the single collision phase space change is not relevant. We have indeed checked that we are in a regime where the phase space of the single scatterings are not relevant by changing the microscopic two-body scattering matrix from anisotropic to isotropic, but renormalizing the total cross section in such a way to keep the same η/s . We have found that leaving unchanged all the other parameters, the elliptic flow is not affected by this change for $p_T \leq 2.5$ GeV, finding some deviations at larger p_T [76]. A similar result is seen if $2 \leftrightarrow 3$ collisions are switched on and off once again the cross sections are such to keep η/s fixed [77].

Once η/s is fixed, we compute the total cross section in each cell of the coordinate space of our grid. To this end we need an analytical relation between η , temperature, cross section and density; as shown in [44, 45], the Chapman-Enskog approximation supplies such a relation with quite good approximation, in agreement with the results obtained using the Green Kubo formula. Therefore, we fix η/s and compute the pertinent total cross section by mean of the relation

$$\sigma_{tot} = \frac{1}{15} \frac{\langle p \rangle}{\rho g(a)} \frac{1}{\eta/s} = \frac{1}{15} \langle p \rangle \tau_\eta, \quad (11)$$

which is valid for a generic differential cross section $d\sigma/dt \sim \alpha_s^2/(t - m_D^2)^2$ as proved in [45]. In the above equation $a = T/m_D$, with m_D the screening mass regulating the angular dependence of the cross section, while

$$g(a) = \frac{1}{50} \int dy y^6 \left[\left(y^2 + \frac{1}{3} \right) K_3(2y) - y K_2(2y) \right] h \left(\frac{a^2}{y^2} \right) \quad (12)$$

with K_n the Bessel function and h corresponding to the ratio of the transport and the total cross section $\sigma_{tr}(s) = \sigma_{tot} h(m_D^2/s)$ and $h(\zeta) = 4\zeta(1+\zeta)[(2\zeta+1)\ln(1+1/\zeta) - 2]$. The $g(a)$ is the proper function accounting for the pertinent relaxation time $\tau_\eta^{-1} = g(a)\sigma_{tot}\rho$ associated to the shear transport coefficient. The maximum value of g , namely $g(m_D \rightarrow \infty) = 2/3$, is reached for isotropic cross section and Eq.(11) reduces to the relaxation time approximation with $\tau_\eta^{-1} = \tau_{tr}^{-1} = \sigma_{tr}\rho$; a smaller value of $g(a)$ means that a higher σ_{tot} is needed to reproduce

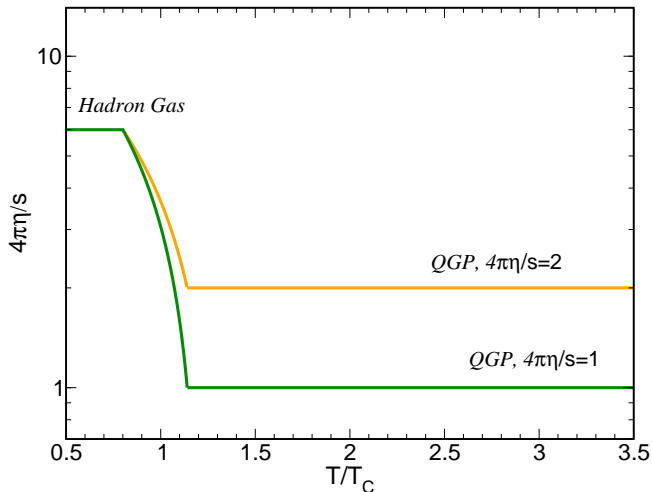


FIG. 2: (color online) Ratio of shear viscosity over entropy density ratio implemented in the present study. Green solid line corresponds to the case in which we take $4\pi\eta/s = 1$ in the quark-gluon-plasma phase, which we then connect smoothly to the value in the hadron phase by means of a kinetic freezeout. For completeness we also show the orange line corresponding to the case $4\pi\eta/s = 2$ in the quark-gluon-plasma phase, which is once again connected smoothly to the value in the hadron phase.

the same value of η/s . However, we notice that in the regime where viscous hydrodynamic applies (not too large η/s and p_T) the specific microscopic detail of the cross section is irrelevant and our approach is an effective way to employ transport theory to simulate a fluid at a given η/s . Therefore from one hand we are in hydrodynamical regime from the other that our approach cannot be and is not meant as a tool to infer a microscopic description of the QGP.

The shear viscosity over entropy density ratio which we use in our study is plot in Fig. 2. In the plasma phase η/s is taken to be a constant, whose numerical value is fixed case by case: in the figure the cases $4\pi\eta/s = 1$ and $4\pi\eta/s = 2$ are represented, but we also perform some simulations with larger values of the ratio. We implement a kinetic freezeout by assuming that η/s increases smoothly in a temperature range from the plasma phase to a hadron phase values which is fixed by referring to the estimates in [80–82]. In this way we take into account scatterings in the hadron phase as well, which however give a very tiny contribution to the collective flow because of the damping due to the larger viscosity and the reduce eccentricity at this later stage.

In the following, we will consider three different types of initial distribution function in the phase-space, which have been considered also in our previous study [21]: two of them are commonly employed in hydro simulations, while the third one represents the novelty of the present study and relies on the ability of the transport approach to include the saturation scale in the initial distribution

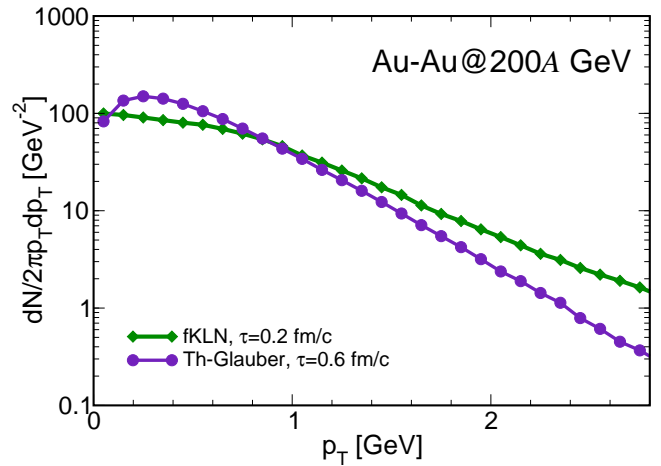


FIG. 3: (Color online) Initial p_T -spectra at midrapidity for the case of a Au-Au collision at $\sqrt{s} = 200$ GeV, with an impact parameter $b = 7.5$ fm.

function, as shown in Fig. 3. For simulations at the RHIC energy we refer to Au-Au collision at $\sqrt{s} = 200$ AGeV; we present here results for $b = 5.2$ fm, $b = 7.5$ fm and $b = 9$ fm. For simulations at the LHC energy we will refer to Pb-Pb collisions at $\sqrt{s} = 2.76$ ATeV, focusing on the case $b = 7.5$ fm.

The standard initial condition for simulations of the plasma fireball created at RHIC is based on the Glauber model, with an \mathbf{x} -space distribution given by the a standard mixture $0.85N_{part} + 0.15N_{coll}$ and a \mathbf{p} -space thermalized spectrum in the transverse plane at a time $\tau_0 = 0.6$ fm/c with a maximum initial temperature $T_0 = 340$ MeV. Following the nomenclature introduced in [21] we will refer to this case as Th-Glauber corresponding to full circles in Fig.3. Within previous studies based on hydro simulations the impact of an initial factorized glasma state has been performed considering an \mathbf{x} -space distribution given by the fKLN (or MC-KLN), while in the momentum space the spectrum has been considered thermalized at $\tau_0 \sim 0.6 \div 0.9$ fm/c [13, 30]; we refer to this case as Th-fKLN; among other things this initial condition, when implemented in hydro simulations, leads to the conclusion that the liquid created by the melting of the glasma is characterized by $4\pi\eta/s \sim 2$ [13, 30, 32] at RHIC, at least for non-central collisions. The third initial conditions is the full fKLN initial conditions where, beyond the \mathbf{x} - space, the saturated distribution in \mathbf{p} -space proper of the model is implemented as well, see Fig. 3 solid thick line with diamonds. We have verified that our main results on thermalization times and elliptic flows are not affected by the choice of τ_0 . In this case as initial time we take $\tau_0 = 0.2$ fm/c with no assumption about thermalization in the transverse plane, as it should the case of any implementation of the KLN model since its proper momentum distribution is out of equilibrium. This initial condition is not usually considered in hydrodynamics because there it is implicitly assumed the

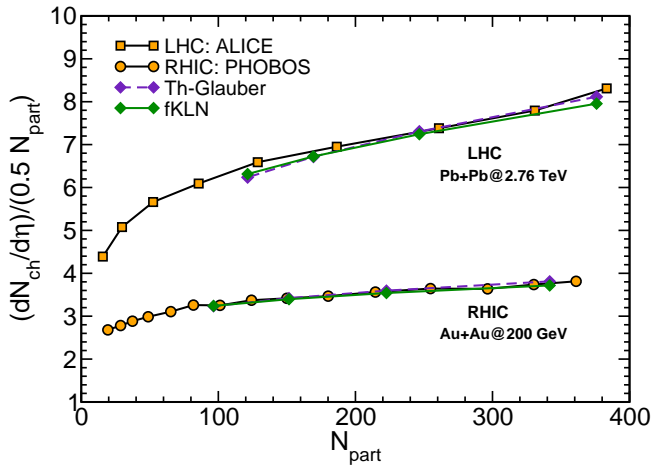


FIG. 4: (Color Online) Multiplicity as a function of N_{part} at RHIC and LHC energies as indicated in the figure. Experimental data are taken from Refs. [87, 88].

system is locally thermalized in the transverse plane, and in fact the initial transverse energy density profile is connected to the initial \mathbf{x} -space fKLN distribution assuming equilibrium thermodynamic relations. In the context of viscous hydrodynamics it is possible to include initial non-equilibrium conditions by introducing an initial non-vanishing value for the viscous tensor $\Pi_{\mu\nu}(\tau_0)$. This has been mostly studied for the shear stress tensor and it has been seen to have a quite small impact on the v_2 at least on the bulk of the system [15, 30, 68]. However the non-equilibrium implied by fKLN implies a change in the trace of the energy-momentum tensor that could be related in hydrodynamical language to a finite bulk stress tensor at τ_0 . To our knowledge it has never been investigated the relation between an initial non vanishing bulk $\Pi_{\mu\nu}(\tau_0)$ and the initial non-equilibrium implied by the saturation scale in the distribution function $f(\mathbf{x}, \mathbf{p})$.

Similarly we introduce Th-Glauber, Th-fKLN and fKLN initial conditions for the LHC runs. In the case of Th-Glauber and Th-fKLN the maximum temperature is taken to be $T_0 = 550$ MeV and the system is assumed to be thermalized in the transverse plane at $\tau_0 = 0.3$ fm/c; for the case of the fKLN initial condition, we keep $\tau_0 = 0.2$ fm/c. This time should correspond to the time interval in which the color strings decay forming the strongly interacting parton liquid.

The particle multiplicity is fixed to correctly reproduce the experimental one for all the three cases. This is shown in Fig. 4 where we plot the particle multiplicity, measured at central rapidity in units of the number of pairs, as a function of the number of participants, for the cases of the fKLN and Th-Glauber initializations. Experimental data are taken from Refs. [87, 88]. In the case of the Th-Glauber and Th-fKLN we have assumed boost invariance in the longitudinal direction for the initial configuration; on the other hand, for the case of the fKLN initial condition a small y -dependence comes from

the distribution in Eq. (3). Nevertheless in both the calculations the total number of particles is the same, as it is shown in Fig. 4.

IV. THERMALIZATION AND ISOTROPIZATION

In Fig. 5 we collect the initial spectra, $dN/2\pi p_T dp_T$, integrated over the momentum rapidity window $|y| < 0.5$, for the case of a Au-Au collision $\sqrt{s} = 200A$ GeV for the fKLN and Th-Glauber initial conditions at their respective initial times τ_0 and at the final time $\tau = 8.2$ fm/c. For the case of the Th-fKLN, we find that the spectra are the same as in the case of the Th-Glauber, therefore we do not plot them in the figure. We have also shown by the dashed line the spectrum at $\tau = 1.2$ fm/c for the case of the fKLN initial condition.

Our main aim is to focus on the impact of the initial conditions implied by the fKLN on the elliptic flow; however we discuss before the time evolution of spectra and the related isotropization. The results in Fig. 5 are obtained with $4\pi\eta/s = 1$. We notice that initially the fKLN spectrum is quite far from a thermalized spectrum; in fact, it embeds the saturation effects which should be proper of the melted glasma. Nevertheless the spectrum thermalizes in the transverse plane within 1 fm/c, since its p_T dependence becomes exponential with a slope very similar to the Th-Glauber.

In the middle panel we compare our results with the experimental data of the STAR collaboration for the charged hadrons [89]. In order to make this comparison we have assumed the quark-hadron duality which implies that for each parton a single hadron is produced; moreover we have multiplied our results by the factor $2/3 \times 3/4$ which takes into account the facts that experimental data correspond to charged hadrons only, and that the rapidity range of experimental data is different from ours. We want only to show that the final spectra between Th-Glauber and fKLN have a very similar shape which make more meaningful the comparison of the elliptic flow discussed in the next Section. The data are mainly shown to have a reference.

In the lower panel of Fig. 5 (c), we have plot the ratio $T^* = E/3N$, evaluated in the local rest frame of the fluid and representing the temperature in the case of a thermalized system, as a function of time. The change of slopes of the curves suggest that initially the cooling of the fireball is dominated by the longitudinal expansion; as soon as the transverse expansion begins ($\tau \sim 2 - 3$ fm/c), the cooling becomes faster and indeed the fireball reaches the freezeout energy density within few fm/c. In the inset of Fig. 5, we plot the quantity $T^* \cdot \tau^{1/3}$. In the case of 1D expansion without dissipation, implies that a thermalized system $T \propto \tau^{-1/3}$. We find that in the case of the fKLN (solid green line) the product $T^* \cdot \tau^{1/3}$ is strongly dependent on time because the system initially is quite far from equilibrium, and the initial

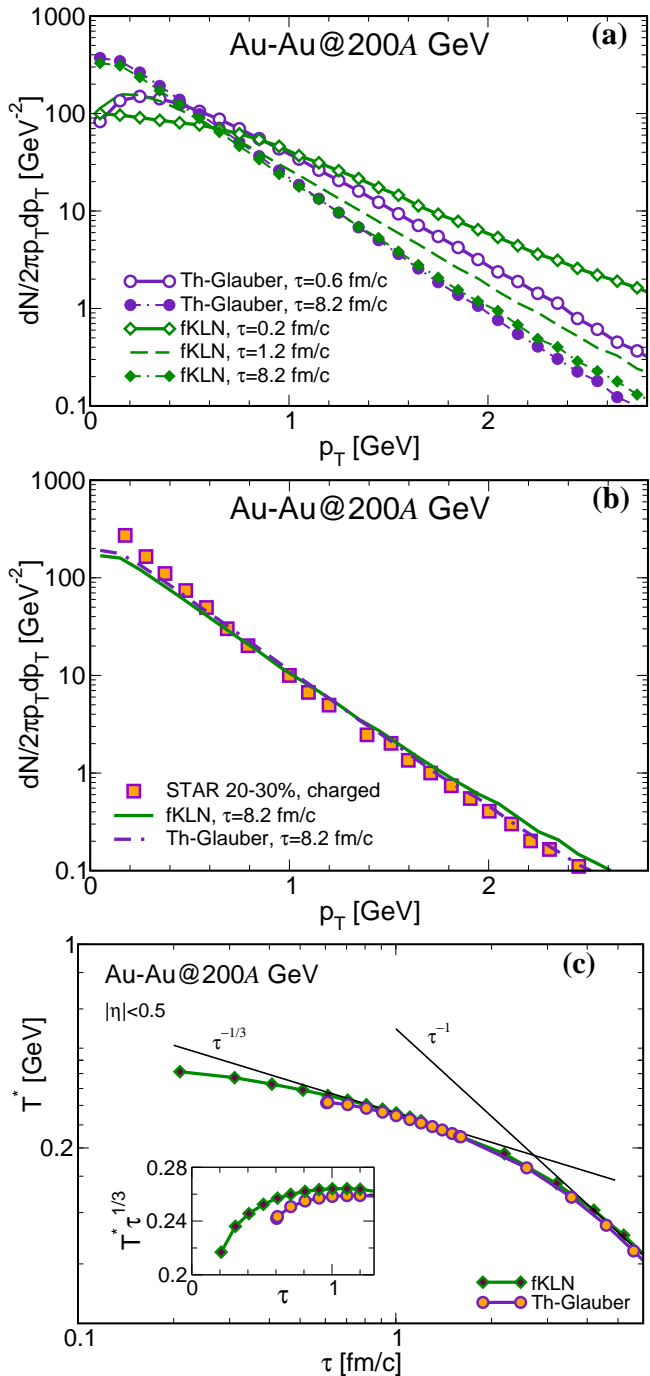


FIG. 5: (Color online) *Upper panel:* Time evolution of spectra. *Middle panel:* Comparison of the final spectra obtained by simulations with experimental data [89]. *Lower panel:* Time evolution of temperature $T = E/3N$. In the inset we plot $T\tau^{1/3}$ for the early stage of the collision. In all panels $b = 7.5$ fm. The Th-fKLN case is not shown because for both spectra and temperature evolution we do not find visible deviations from the Th-Glauber initialization.

non-equilibrium generates some entropy to thermalize; however at $\tau \sim 0.8$ fm/c we find $T^* \cdot \tau^{1/3}$ saturates to a

constant value, signaling the system has thermalized in the whole momentum space. We notice a tiny evolution also for these cases that we have indicated as thermal. The reason is that the initial spectra are thermal only in the transverse plane, while they are boost-invariant along the longitudinal direction. Furthermore as one can expect by solving the Boltzmann under boost invariance at mid-rapidity T^* should decrease as $\tau^{-\delta}$ with $\delta = P_L/\epsilon$ that is smaller than $1/3$ [90]. This causes a tiny evolution to the constant value, that would disappear when the distribution is thermal also in the longitudinal direction. At larger times T^* decreases faster because the 3D expansion sets in and at $\tau \sim 2 - 3$ fm/c one has $T^* \sim \tau^{-1}$ as shown in the main panel of Fig. 5 with the thin solid line indicating the τ^{-1} behavior. We remark that even if we have chosen to start our simulation at $\tau_0 = 0.2$ fm/c, our final result on thermalization time required by the KLN initial condition is unaffected if we shift the initial time to a reasonably larger value.

A posteriori our results on short thermalization times are quite natural: in fact, we have assumed the fluid expands with a very small shear viscosity, which naturally implies that the coupling among the partons are nonperturbative, hence leading efficiently the distribution to the fixed point of the Boltzmann equation, namely a thermalized distribution. These results on fast thermalization are in agreement with earlier studies showing that two-body collisions are insufficient to achieve a fast thermal equilibrium [46], and three-body processes are necessary. In fact in that case the perturbative QCD two-body cross section is used, which corresponds to η/s about one order of magnitude larger than in our case; hence, to achieve fast thermalization three-body processes have to be fed into the collision integral. The difference with [46] is that we do not focus on the microscopic details which lead to thermalization, as discussed in Section III: we are interested to simulate the dynamics of a fluid with few macroscopic properties specified, namely the equation of state and the ratio η/s . Thus we normalize the cross section locally to get the wanted η/s , and our scattering rates even if obtained effectively by two-body scattering are very large, leading eventually to a fast thermalization.

In Fig. 6, we plot our results for the spectra for a Pb-Pb collision at $\sqrt{s} = 2.76A$ TeV, corresponding to a typical LHC collision. As expected, the qualitative behaviour of spectra is unchanged shifting from the RHIC to the LHC energy. In this case however the effect of the saturation scale is smaller, because the initial temperature for the Th-Glauber initial condition is larger, as it can be inferred from the spectra. Hence the p_T -spectra for the thermalized case is indeed quite close to the fKLN one, as shown in Fig.6 (upper panel). Also in the case of the Pb-Pb collision, starting from $\tau_0 = 0.2$ fm/c for the fKLN melted glasma initial condition, time evolution of spectra shows that the transverse thermalization occurs within $\Delta\tau \approx 1$ fm/c. At LHC the time scale at which $T^* \cdot \tau^{1/3}$ is constant appears to be quite similar to the one at RHIC in Fig.5 (c).

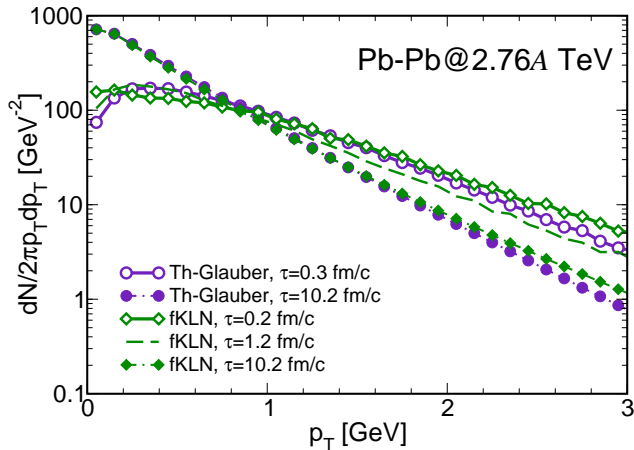


FIG. 6: (Color online) Time evolution of spectra at midrapidity for Pb-Pb collision at $\sqrt{s} = 2.76A$ TeV, with an impact parameter $b = 7.5$ fm.

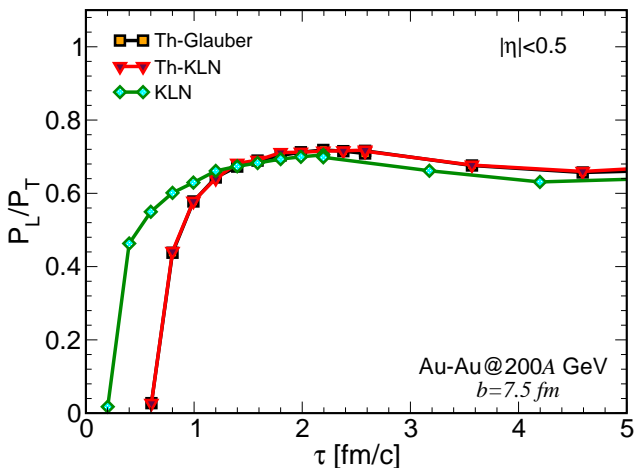


FIG. 7: (Color online) Time evolution of the ratio P_L/P_T , for several initial conditions. Upper panel results refer to Au-Au collisions at $\sqrt{s} = 200A$ GeV.

We have studied also the isotropization of pressures for the expanding system. The energy-momentum tensor is defined locally as

$$T^{\mu\nu}(x) = \int \frac{d^3\mathbf{p}}{(2\pi)^3} \frac{p^\mu p^\nu}{E} f(x, p), \quad (13)$$

where f corresponds to the invariant distribution function. In our simulations the energy-momentum tensor is defined in each cell and it is computed in the local rest frame of the fluid, subtracting the radial flow contribution; we then define locally transverse and longitudinal pressures, P_T and P_L respectively, as

$$P_T(x) = \frac{T_{xx}(x) + T_{yy}(x)}{2}, \quad (14)$$

$$P_L(x) = T_{zz}(x); \quad (15)$$

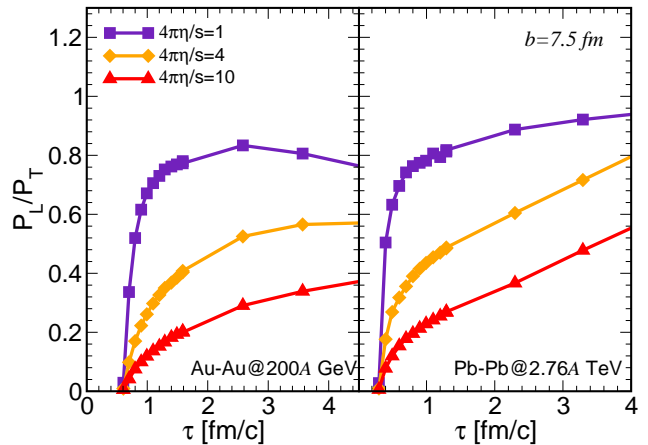


FIG. 8: (Color online) Time evolution of the ratio P_L/P_T , for the case of the Th-Glauber initial condition, for several values of the ratio η/s . Left panel corresponds to Pb-Pb collision at $\sqrt{s} = 2.76A$ TeV; right panel corresponds to Au-Au collision at $\sqrt{s} = 200A$ GeV. Selection in transverse plane is $|R_T| < 2$ fm and space-time rapidity $|\eta| < 0.5$. All the calculations refer to collisions with an impact parameter $b = 7.5$ fm.

finally we average P_L/P_T over several cells in order to lower the effect of statistical fluctuations. In Fig. 7 we plot our results about P_L/P_T as a function of time, for several initial conditions and for the case of strong coupling $4\pi\eta/s = 1$. In particular in the figure we have averaged over a square in the central region of the transverse plane whose side is of 2 fm, while in the longitudinal direction we have averaged over $|\eta| < 0.5$. At early times the longitudinal pressure is zero due to the Bjorken initial conditions. Our findings suggest that independently on the initial condition implemented, the system becomes nearly isotropic ($P_L/P_T \sim 0.7$) within a $\Delta\tau_{isotr} \sim 0.5$ fm/c for $4\pi\eta/s = 1$.

We have selected the region $|\eta| < 0.5$ checking that the particle in this space region are nearly correspondent to all the particles with momentum rapidity $|y| < 1$ to which we are mainly interested. We have also checked that the maximum value of P_L/P_T marginally depends on the space region selected while its maximum values increase up to $P_L/P_T \sim 0.8$ if one selects the central region (see also Fig.8), while it goes down to $P_L/P_T \sim 0.6$ if one considers the entire fireball in both transverse and longitudinal direction. A similar behavior is observed at LHC as can be seen for the Th-Glauber case also in the left panel of Fig.8.

It is interesting to compute how the isotropization is affected by the η/s of the fluid. To this end in Fig. 8 we show our results for pressures at the RHIC (right panel) and LHC (left panel) energies, for the Glauber initial condition (for the fKLN initial condition we obtain similar results), for different values of the ratio $4\pi\eta/s$. In particular, the value $4\pi\eta/s = 10$ corresponds approximately to the perturbative QCD estimate [44, 45, 83].

As expected, the larger the η/s , the smaller the ability of the system to remove the initial pressure anisotropy and a perturbative fluid would not be able to sufficiently isotropize the pressure. The ratio P_L/P_T reaches its maximum value slowly as η/s increases: turning from $4\pi\eta/s = 1$ to $4\pi\eta/s = 10$ the capability of the system to reach isotropization is lost while it is barely reached for $4\pi\eta/s \sim 0.3$ but $\Delta\tau_{isotr} \approx 3$ fm/c. At LHC the trend is similar but the larger density to reach slightly larger values of P_L/P_T .

Similar results on incomplete isotropization have been found in [52], where Schwinger mechanism causes the color strings decaying into a parton liquid and shear viscosity is taken into account via the relaxation time ansatz. Respect to [52] we consider a full 3D+1 simulation and we do not employ the relaxation time approximation, solving the kinetic equation with the full Boltzmann integral. On the other hand, we miss the field dynamics that causes oscillations of P_L/P_T which in the early phase generates a peak in the P_L/P_T at $\tau \sim 1$ fm/c and in 3D+1 could also lead to instabilities in three dimensions in the very early stage of the expansion.

The results in Fig. 7 and 8 are comparable with previous calculations [52, 53] in which a dynamics for the color glasma fields is introduced; this comparison is quite meaningful because it is well known that in the very initial stage of its dynamics, the glasma is characterized by $P_L < 0$ due to strong fields in the longitudinal direction. This negative pressure cannot be reproduced within our simulation code at the moment because we have not yet implemented a dynamics for the classical chromoelectric and chromomagnetic fields. Nevertheless as shown in [52, 53] the ratio P_L/P_T becomes positive within $\tau_+ \approx 0.1 \div 0.2$ fm/c depending on the coupling strength, and unless the system is in weak coupling the strength of the fields becomes negligible for $\tau > \tau_+$ [52], which justifies our assumption that starting the simulations at $\tau = \tau_0 = 0.2$ fm/c the evolving fireball can be described by a parton liquid with positive pressure.

V. ELLIPTIC FLOW

The main goal of our study is the computation of the differential elliptic flow for different initial conditions, both at RHIC and LHC energies. The main motivation has been discussed in the first part of Section III.

Before discussing the elliptic flow we show the results obtained for the momentum eccentricity,

$$\varepsilon_P = \frac{\langle T_{xx} \rangle - \langle T_{yy} \rangle}{\langle T_{yy} \rangle + \langle T_{xx} \rangle}, \quad (16)$$

which is usually computed also in hydrodynamics [70–73] and whose evolution is not related to the freezeout by the Cooper-Frye hypersurface as instead happens for v_2 . The average in the above equation is understood in the transverse plane at midrapidity. We compute this quantity to show that especially for the bulk of the system the kinetic

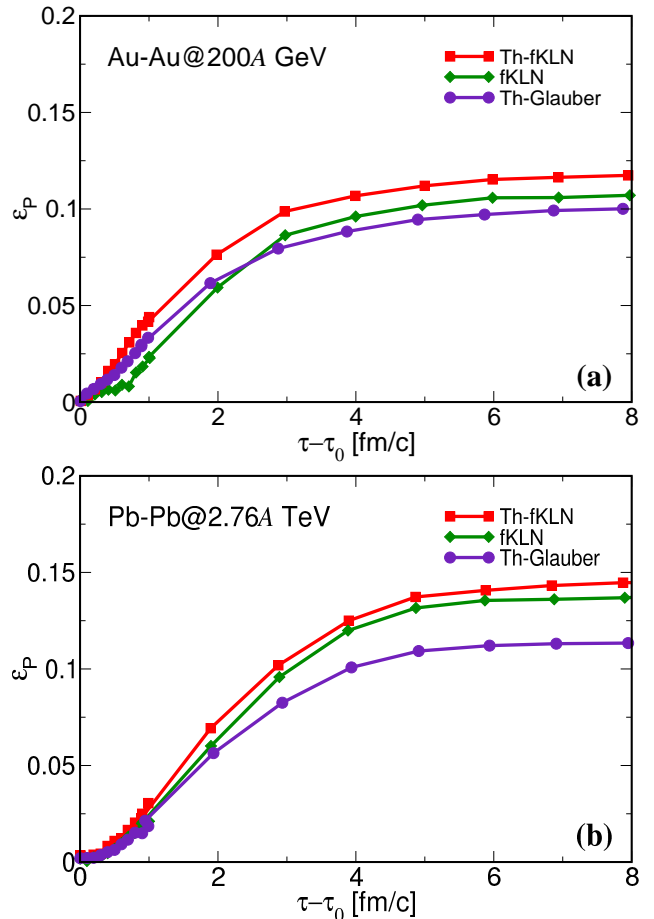


FIG. 9: (Color online) Momentum eccentricity, ε_P , as a function of time for three different initial conditions. Upper panel refers to Au-Au collisions at $\sqrt{s} = 200A$ GeV; lower panel to Pb-Pb collisions at $\sqrt{s} = 2.76A$ TeV. In all calculations the impact parameter $b = 7.5$ fm, $4\pi\eta/s = 1$. Components of the energy-momentum tensor have been integrated over $|\eta| < 0.5$. For the fKLN initial condition we have chosen $\tau_0 = 0.2$ fm/c, while for the thermal distributions $\tau_0 = 0.6$ fm/c.

Boltzmann approach determines a hydro-like evolution. In Fig. 9, we plot the momentum eccentricity as a function of time, for the three different initial conditions we study in this article, for both RHIC and LHC energies. For completeness in Fig. 10 we plot the space eccentricity ε_x as a function of time for the cases of collisions at RHIC (upper panel) and LHC (lower panel) energies. Results in Fig. 9 show that momentum anisotropy is built-up within the first few fm/c, which means that the elliptic flow is being developed in the same time range. However, in this time range ε_x in the case of the fKLN initial condition is comparable to that of the Th-fKLN. Eventually the system enters the freezeout and almost free streaming regime, and the ε_x for the two cases evolve in a different way. This suggests that when the major part of the momentum anisotropy is formed, the fireball expands in the transverse plane almost in the same way both in the

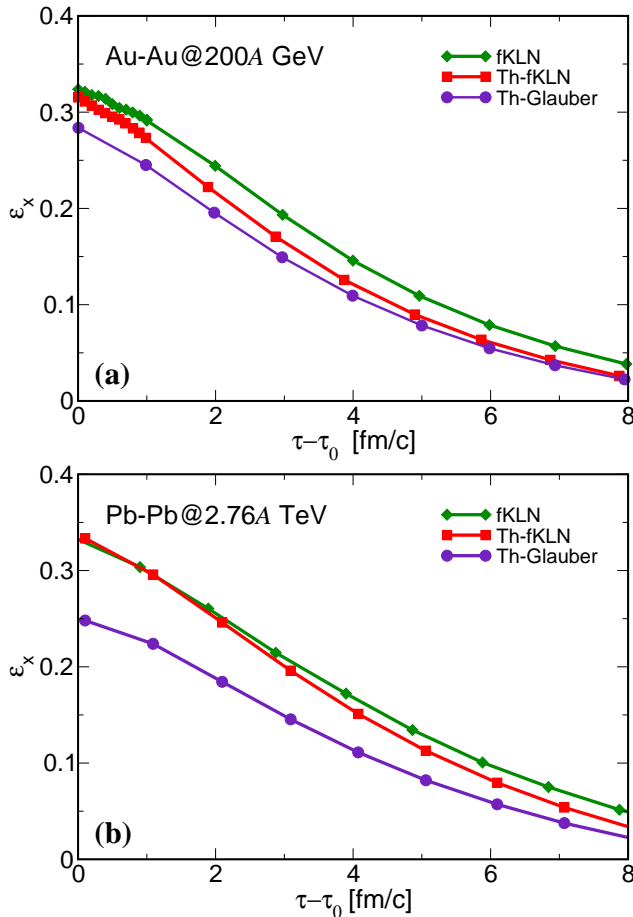


FIG. 10: Time evolution of eccentricity, for the cases of a Au-Au collision (upper panel) at $\sqrt{s} = 200A$ GeV, and of a Pb-Pb collisions at $\sqrt{s} = 2.76$ TeV. In all calculations the impact parameter $b = 7.5$ fm and $4\pi\eta/s = 1$. For the fKLN initial condition we have chosen $\tau_0 = 0.2$ fm/c, while for the thermal distributions $\tau_0 = 0.6$ fm/c.

Th-fKLN and in the fKLN cases; therefore the difference in elliptic flow in the two cases has to be generated mainly by the different momentum distribution in the initial stage.

Our results on ε_P are in fair agreement with those obtained within hydro simulations [70, 71]. A strict quantitative comparison with the aforementioned results is not feasible because the results in [70, 71] are obtained using simulations in 2+1 dimensions with some differences in the initial temperature and density profile and a different temperature dependence of the hadron gas shear viscosity and also a different freezeout temperature. Even with these differences we can compare our results with those of the EOS I case (perfect gas EoS) in [71], see their Fig. 2. The time evolution of ε_P has some difference in the two cases, in particular in our case it grows faster with time, which is likely due to the differences mentioned above, nevertheless the asymptotic value are in good agreement with the Th-Glauber case.

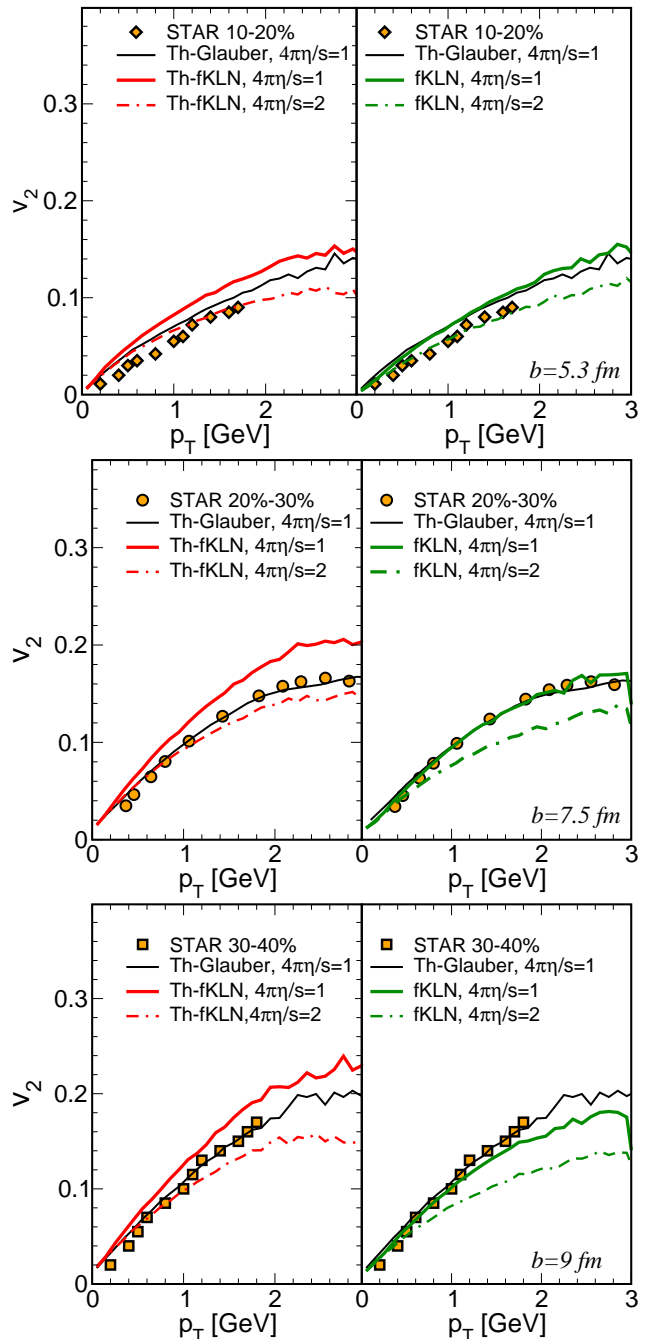


FIG. 11: (Color online) Elliptic flow $v_2(p_T)$ at midrapidity $|y| < 0.5$ for different initial conditions and η/s as in the legend. All the calculations refer to Au-Au collisions at $\sqrt{s} = 200$ GeV. From the upper to the lower panel the impact parameter $b = 5.3$ fm, $b = 7.5$ fm and $b = 9$ fm respectively.

In Fig. 11, we collect our results for the differential elliptic flow for the case of a Au-Au collision at $\sqrt{s} = 200A$ GeV, with three different impact parameters: from the upper to the lower panel the impact parameter is $b = 5.3$ fm, $b = 7.5$ fm and $b = 9$ fm respectively. The case $b = 7.5$ fm corresponding to the 20 – 30% centrality class

at RHIC has been already considered in [21], but with a different value of Q_0 : here $\langle Q_0 \rangle \approx 1$ GeV in the transverse plane at $x = 0.01$, while $\langle Q_0 \rangle \approx 1.4$ GeV in [21]. We have used a different value of Q_0 in the present calculations mainly because in this way we do not need to manipulate other parameters, among them the initial temperature as well as the T dependence of η/s in the cross-over region that regulates the kinetic freeze-out temperature, in order to obtain final spectra which are in agreement among the different initial conditions; moreover we want to check that within a reasonable uncertainty on $\langle Q_s \rangle$ the effect we measure on the elliptic flow persists.

Spectra corresponding to these data are plot in Fig. 5 for the case $b = 7.5$ fm (for the other values of b we obtain similar results). In Fig. 11 we have split the results for each value of b into two panels: the left one corresponds to our hydro-like calculations, in which the initial distribution is assumed to be thermalized in the transverse plane. On the right panel we plot the results obtained assuming the nonequilibrium distribution in the initial condition. To guide the eye, in the figure we also plot experimental data for v_2 in the relevant centrality class from the STAR collaboration [69]. The $v_2(p_T)$ from the kinetic simulations are quite close to the data for the Th-Glauber and fKLN initializations with $4\pi\eta/s = 1$. However we remind that no hadronization process is yet included in our approach, so the agreement with the charged hadrons has to be taken with caution even if it indicates that the azimuthal asymmetries generated are in the right ball park.

The Glauber initial condition is in agreement with experimental data for $4\pi\eta/s = 1$; instead, in the case of Th-fKLN the elliptic flow for the same value of η/s overshoots data except for very central collisions: in order to reproduce better experimental data one, η/s has to be increased by about a factor of two. These results are in agreement with the ones obtained from viscous hydrodynamics [13, 30, 32], showing the solidity and consistency of our transport approach at fixed η/s . The necessity of a larger η/s to reproduce data on elliptic flow is usually understood in terms of the larger initial eccentricity of the Th-fKLN fireball compared to the Glauber one, which would result in fact in a larger anisotropy in momentum space unless viscosity is large enough to damp the flow [13, 30, 50].

In the right panel of Fig. 11, we present the result for the fKLN model, when the proper distribution function is implemented in both the \mathbf{x} and \mathbf{p} spaces. We find that fKLN with a $4\pi\eta/s = 1$ gives a $v_2(p_T)$ quite similar to the Th-Glauber, even if the initial eccentricity in this case is the same as the one of the Th-fKLN case. For fKLN with $4\pi\eta/s = 2$ the differential elliptic flow would be too small. In other words the initial out-of-equilibrium fKLN distribution reduces the efficiency in converting ϵ_x into v_2 . Our interpretation is that the initial large eccentricity of the fKLN configuration is compensated by the key feature of an almost saturated initial distribution in \mathbf{p} -space below the saturation scale Q_s and probably by the

softer tail at $p_T > Q_s$. We notice that changing the centrality class we have found that the effect of the initial distribution on the elliptic flow becomes smaller as we turn from peripheral to central collisions, as it can be seen in Fig. 11. We obtain similar results at the LHC energy, Fig. 12, where we collect the results of our computation of $v_2(p_T)$ for $b = 7.5$ fm and for $Q_0 = 1$ GeV (upper panel) and $Q_0 = 2$ GeV (lower panel), in order that $\langle Q_s \rangle$ is in agreement with the estimates of [57]. We can see that the Th-fKLN overestimate the $v_2(p_T)$ at both $4\pi\eta/s = 1$ and 2 and probably even a $4\pi\eta/s \sim 3$ is needed to account for the data. When the full fKLN is implemented we can see that the damping effect already discussed at RHIC is such that with an $4\pi\eta/s = 2$ one predicted a $v_2(p_T)$ quite close to experiments.

This result we measure on the elliptic flow can be understood naively connecting v_2 to the slope of the spectrum, which corresponds to the inverse temperature if the spectrum is a thermal one. In fact, the elliptic flow can be understood as a larger slope of the momentum spectrum in the out of plane \vec{x} direction respect to the \vec{y} one caused by a larger pressure in the \vec{x} direction due the elliptical shape. The net effect in terms of the difference of the particle yields between the two directions is larger if the spectra are decreasing exponentially respect to the case in which they are nearly flat as a function of p_T .

In Fig. 13 we plot the differential elliptic flow at $p_T = 2$ GeV for different initializations, as a function of the number of participants. We have shown results for $b = 2.5$ fm corresponding to $N_{part} = 352$, $b = 5.3$ fm corresponding to $N_{part} = 245$, $b = 7.5$ fm corresponding to $N_{part} = 154$ and $b = 9$ fm corresponding to $N_{part} = 104$. This comparison is meaningful since it permits to visualize and summarize the dependence of $v_2(p_T)$ on the centrality class, comparing the impact of the initial distribution on the final v_2 . In particular the discrepancy between Th-fKLN and fKLN initializations becomes less relevant for more central collisions, implying that the effect of the initial momentum distribution is not negligible if one considers non-central collisions. We also note that for central collisions at RHIC Th-Glauber and Th-fKLN for $4\pi\eta/s = 1$ predict the same v_2 and the effect is of KLN generating larger v_2 disappears. This is seen also in viscous hydro simulation and it is a further confirmation that our approach converge to viscous hydro when the same thermal initial conditions are employed.

In Fig. 14, we plot the elliptic flow as a function of time for particles at $p_T = 1.5$ GeV. Both the cases of the RHIC and LHC runs are shown in the figure, for non-central collisions with $b = 7.5$ fm. In the figure we plot quantities as a function of $\tau - \tau_0$ rather than τ , where τ_0 is the time at which dynamical evolution begins, because anisotropy is formed thanks to particle interactions which are effective at $\tau \geq \tau_0$. In the case of RHIC the behavior clearly splits into two classes: one is represented by the thermal distributions; the other one is given by the case in which the initial spectrum is the fKLN one. In the case of LHC this distinction is quantitatively less

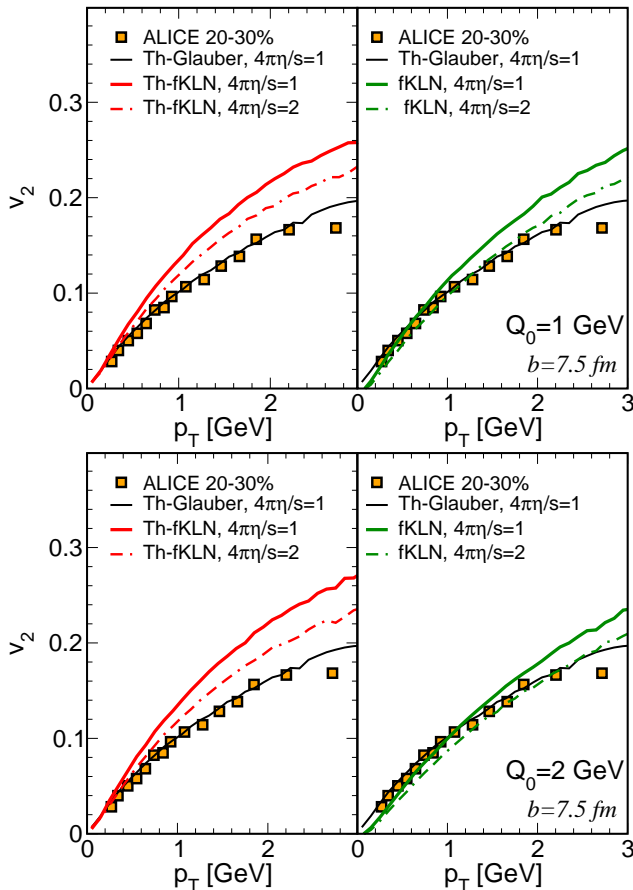


FIG. 12: (Color online) *Upper panel.* Elliptic flow $v_2(p_T)$ for the different initial conditions and η/s as in the legend, for the case $Q_0 = 1$ GeV where Q_0 is defined in Eq. (7). *Lower panel.* Same quantity for $Q_0 = 2$ GeV. All the calculations refer to Pb-Pb collisions at $\sqrt{s} = 2.76$ TeV, with an impact parameter $b = 7.5$ fm.

relevant but still present, probably because as already said the difference between the thermal distribution and the KLN one is less pronounced.

The main point which we emphasize is that $dv_2/d\tau$ for the thermal distributions is large from the very beginning of the dynamical evolution, while it is quite reduced for fKLN. This is a further clue that the initial distribution is very important for the build-up of v_2 , a statement that we have already supported discussing the evolution of eccentricities and momentum anisotropy. We further note that for $\tau - \tau_0 \geq 1$ fm/c, which is the time range roughly corresponding to the thermalization time for all the cases considered here, $dv_2/d\tau$ of fKLN becomes very similar to Th-fKLN and Th-Glauber. This observation further confirms that it is the initial out-of-equilibrium and nearly saturated distribution that dampens the efficiency in converting the space eccentricity into the v_2 . Therefore, even if thermalization sets in quickly, as assumed in hydrodynamics $\tau_{isotr} \sim 0.8$ fm/c, the actual evolution from the initial state to the thermalized one

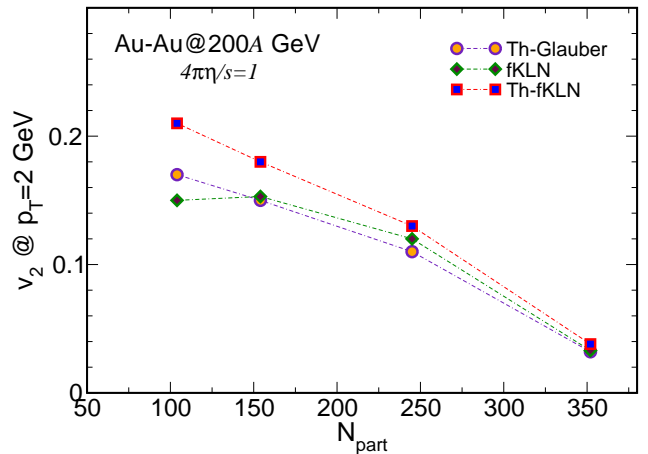


FIG. 13: Elliptic flow $v_2(p_T)$ at midrapidity $|y| < 0.5$ and at $p_T = 2$ GeV for different initial conditions, computed at $4\pi\eta/s = 1$. All the calculations refer to Au-Au collisions at $\sqrt{s} = 200$ GeV.

cannot be neglected in studying the elliptic flow, especially at RHIC energy where most of the anisotropy in momentum space develops in the first 3 fm/c at least for semi peripheral collisions.

VI. INVARIANT DISTRIBUTION FUNCTIONS

Before going to the conclusions we want to discuss the range of values covered by the phase space distribution functions. This is an issue that recently has attracted a particular interest because it could be possible that with the high density reached in the initial stage of the collision the bosonic quantum nature of gluons triggers a Bose-Einstein condensation [48]. The invariant distribution function, f , is defined as

$$f = \frac{(2\pi)^3}{g} \frac{\Delta N}{\Delta^2 \mathbf{x}_\perp \Delta^2 \mathbf{p}_T \Delta z \Delta p_z}, \quad (17)$$

where N counts the number of particles in the phase space volume given by $\Delta^2 \mathbf{x}_\perp \Delta^2 \mathbf{p}_T \Delta z \Delta p_z$ and $g = 8 \times 2$ corresponds to the number of gluonic degrees of freedom. On our grid we have $\Delta^2 \mathbf{x}_\perp = \delta_{cell}^2 = 0.4$ fm² and $\Delta z = \tau \eta_{cell}$; moreover, we take $\Delta^2 \mathbf{p}_T = p_T \Delta p_T \Delta \phi$ and we sample the momentum space with $\Delta p_T = 0.1$ GeV. We integrate over momentum rapidity: this is necessary since at initial time $\tau = \tau_0$ we assume $y = \eta$, which implies the initial distribution to be singular, namely

$$f = \tilde{f}_0 \delta(y - \eta), \quad \tau = \tau_0; \quad (18)$$

the subscript 0 reminds that the above equation is valid only at $\tau = \tau_0$. Because of the delta-function the measurable quantity at $\tau = \tau_0$ is \tilde{f}_0 , which can be obtained by integrating f over momentum rapidity; when we compute the distribution function at later times, for consistency

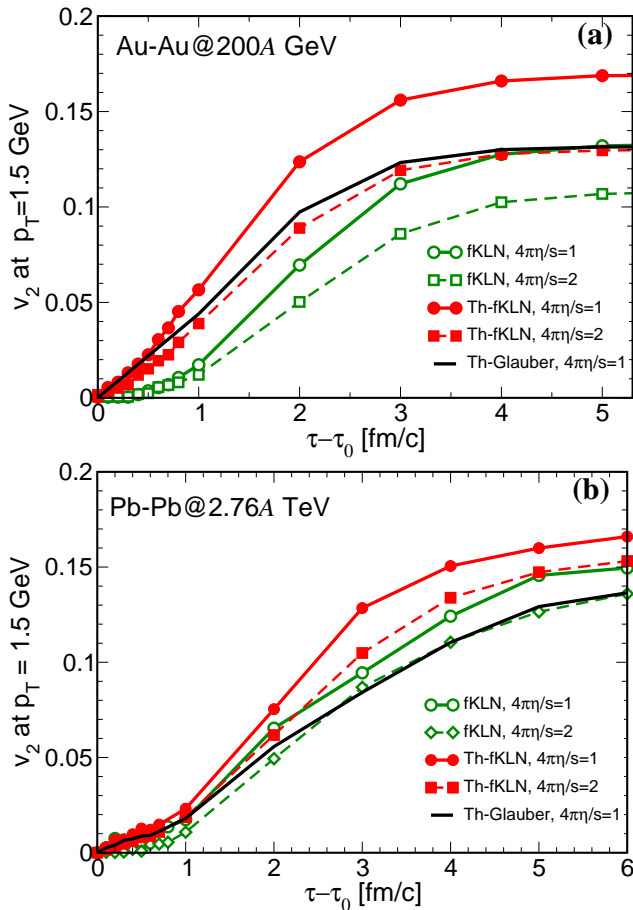


FIG. 14: (Color online) Evolution of v_2 at $p_T = 1.5$ GeV as a function of the evolution time for all the different initial conditions and η/s values. Upper panel refers to Au-Au collisions at $\sqrt{s} = 200$ GeV, with an impact parameter $b = 7.5$ fm. Lower panel corresponds to Pb-Pb collisions at $\sqrt{s} = 2.76$ TeV, with an impact parameter $b = 7.5$ fm.

we also integrate over momentum rapidity. For later convenience we also integrate over the azimuthal angle ϕ . We then define

$$\langle f \rangle = \frac{1}{2\pi} \int d\phi \int f dy, \quad (19)$$

which on each cell of the configuration space reads

$$\langle f \rangle = \frac{1}{2\pi\tau} \frac{1}{\eta_{cell}\delta_{cell}^2} \sum_{cell} \frac{1}{E p_T \Delta p_T}, \quad (20)$$

with $E = \sqrt{p_z^2 + \mathbf{p}_T^2} = p_T \sqrt{1 + \sinh^2 y}$ and the sum is understood over all the particles that at time τ are in the specified cell.

Here we present the evolution of $f(p_T)$ in the central region of a QGP fireball to have a first estimate of the value explored with time and transverse momentum p_T . In Figs. 15 and 16 we plot the invariant distribution functions for two different initial conditions. The upper

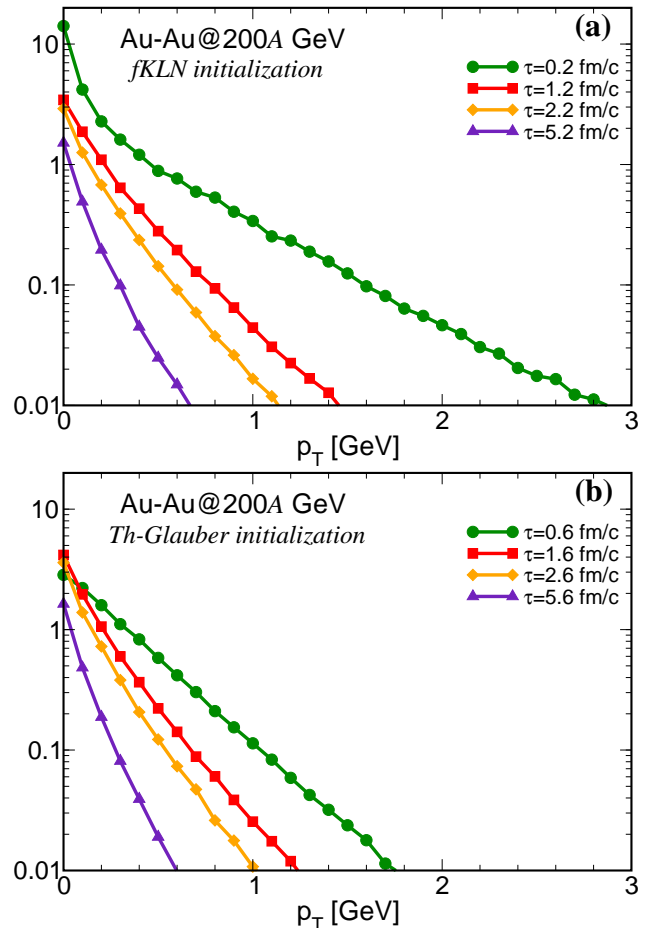


FIG. 15: (Color online) *Upper panel*: Invariant distribution function for several times, for the case of the fKLN initial condition. *Lower panel*: Same quantities computed for the Glauber initial condition. All the calculations refer to Au-Au collisions at $\sqrt{s} = 200A$ GeV, with an impact parameter $b = 7.5$ fm and $4\pi\eta/s = 1$.

panels of the figures correspond to the fKLN, while the lower panels correspond to the Glauber initial condition; Fig. 15 is the result for the Au-Au collisions at the RHIC energy, while Fig. 16 corresponds to the case of Pb-Pb collisions at the LHC energy. In order to obtain the results shown in the figure, we have integrated Eq. (20) over the region $|x_T| < 2.45$ fm, $|y_T| < 4.55$ fm and $|\eta| < 0.1$, which embed the hottest and densest parts of the initial fireball. However, the results are qualitatively similar if we chose to compute $\langle f \rangle$ by means of Eq. (20) only in the central cell. The natural consequence of the longitudinal (as well as the transverse) expansion is that the distribution function becomes smaller and smaller as time increases. In fact, from Eq. (20) we expect $f \sim \tau^{-1}$ due to the longitudinal expansion close to luminal velocity.

In Fig.16 (upper panel) we can observe that at $p_T \sim 1$ GeV the initial $\langle f(p_T) \rangle \sim 0.5$ but the rapid longitudinal expansion along with the rapid cooling down is such

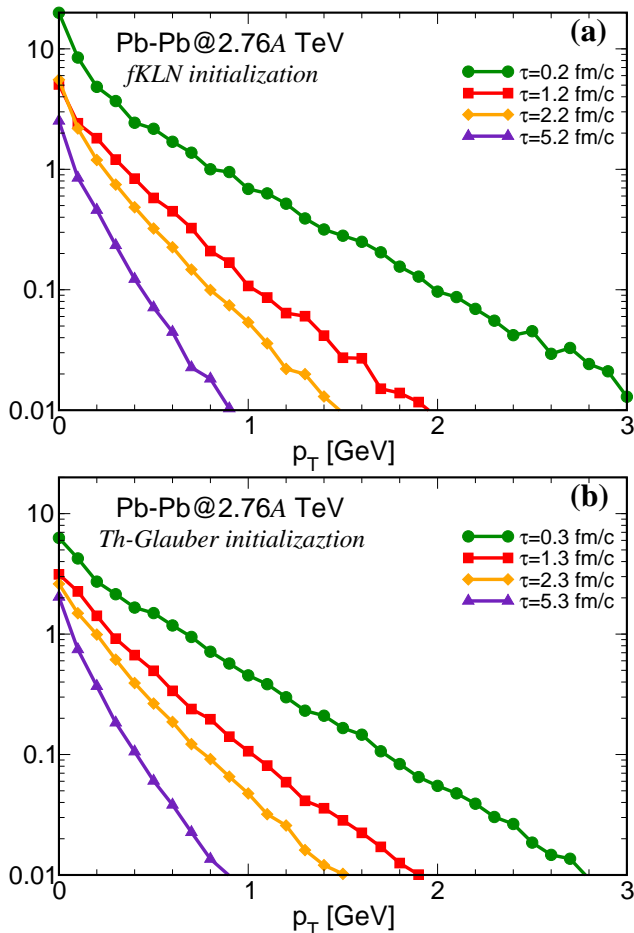


FIG. 16: (color online) *Upper panel:* Invariant distribution function for several times, for the case of the fKLN initial condition. *Lower panel:* Same quantities computed for the Glauber initial condition. All the calculations refer to Pb-Pb collisions at $\sqrt{s} = 2.76A$ TeV, with an impact parameter $b = 7.5$ fm and $4\pi\eta/s = 1$.

the f decreases very quickly with and at $\tau \sim 1$ fm/c it is already smaller than $5 \cdot 10^{-2}$. On the hand at $p_T < 0.5$ GeV not only at τ_0 the $\langle f(p_T) \rangle > 1$ but due to the high scattering rates that drive a rapid thermalization the decrease of $\langle f(p_T) \rangle$ with τ^{-1} is fully damped at even at $\tau \sim 1 - 2$ fm/c we have $\langle f \rangle \sim 1$. A similar trend with even larger value of $\langle f \rangle$ is observed at LHC and not only for the fKLN but also for the Th-Glauber initial conditions.

We remind that in our formulation we have not introduced the bosonic enhancement factors in the collision integral, which however are expected to give a relevant effect if $f \gtrsim 1$. Still our result shows that the longitudinal expansion coupled to the thermalization process keeps the occupation number quite large for a relatively long time interval and therefore it is reasonable to expect that the formation of a transient Bose-Einstein condensate also in the expand glasma in HIC and not only for

the static case of a system in a box [48]. The results of [48] are of course quite interesting and we plan to improve our calculation in the near future to take into account the Bose enhancement factors in the collision integral, as well as the inelastic processes which convert gluons to quarks.

As for the effect discussed on the build-up of v_2 in Section IV, we do not expect significant impact of the Bose-Einstein enhancement factors $1 + f$ in the collisions integral because, as discussed, only for small p_T , f is relatively large and furthermore only in the very central region of the fireball. while our effect take place for $p_T > 1$ GeV. Moreover, the effect we find is mainly due to the initial non-equilibrium dynamics and not to the fixed point of the kinetic equation which instead determines the final state. Further investigations are in progress.

VII. CONCLUSIONS

In this article we have presented our results on thermalization, isotropization and building-up of the elliptic flow for fireballs produced in relativistic heavy ion collisions both at RHIC and LHC energies. We have put emphasis on the role of a nonequilibrium initial condition on the generation of the collective flow, using as a model the fKLN-glasma initial condition which differs from the thermal distribution for the presence of a saturation scale in the low p_T spectrum. Our study is based on kinetic theory at fixed η/s .

In our study we have neglected the initial time evolution of the chromo-electric and chromo-magnetic fields (the glasma) produced immediately after the collision, whose intensity can be directly related to the saturation scale Q_s in the CGC before the collision. Therefore our approach could be justified as soon as the initial strong glasma longitudinal fields decay into particle quanta and its longitudinal pressure becomes positive. The characteristic time for this decay is of the order of $\tau_0 \approx 1/Q_s$ [52–54]. The advantage to use kinetic theory from τ_0 rather than hydro is that the nonequilibrium initial distribution is not problematic as kinetic theory is built to study the evolution of a generic $f(x, p)$ distribution function.

As a non-equilibrium initial distribution in our simulations we have used the spectrum obtained within the fKLN model, which embeds a saturation scale in momentum space. In both RHIC and LHC runs we have found that thermalization times are $\Delta\tau_{therm} \sim 0.8-1$ fm/c. Moreover we have studied the time scales for the isotropization of the expanding fireball, defining transverse and longitudinal pressures, P_T and P_L respectively, and computing the time evolution of P_L/P_T . We have found that isotropization is not reached if $\eta/s \geq 0.3$, in agreement with [52, 53]; this result is easily understood, since higher viscosity implies lower cross sections among partons and dynamics in the longitudinal direction and transverse plane are decoupled. On the other hand it is

significant that for a fluid with $\eta/s \sim 0.1$ also isotropization ($P_L/P_T \simeq 0.7$) occurs very quickly $\tau \sim 0.5$ fm/c.

We have then focused our attention on the elliptic flow production when the initial distribution has a saturation scale built in it. We have found that the amount of elliptic flow produced in heavy ion collisions depends not only on the pressure gradients and the η/s of the system, but also on the initial distribution in momentum space. In particular, an initial condition characterized by a momentum distribution with a saturation scale generates smaller v_2 respect to the thermal one. This result is quite general, and we expect it should be valid, besides QGP in uRHICs, for systems like cold atoms in a magnetic trap which are characterized by a value of η/s close to the QGP one [47]. Assuming the fKLN distribution as the one arising from the melting of the glasma, the effect of the initial nonequilibrium distribution affects the estimate of η/s of about a factor of two. However we have seen also that this effect is maximal for semi-peripheral collisions, becoming quite small for very central collisions.

The relevance of our results is further enhanced by the fact that Th-fKLN with $4\pi\eta/s \sim 2$ would generate a low v_3 respect to the available data. This is the main conclusion of [32], namely that Th-fKLN is not able to describe for the experimental observations, might be revised.

In order to make more precise comparison with experimental data we are currently implementing also fluctuating initial conditions which will allow to extend the present study to all the v_n harmonics relevant in HIC's. This will allow to see if fKLN can account for the measured v_3 or the non-equilibrium damps such harmonics even more than what seen in hydrodynamics. In [51] it is found that harmonics up to the fifth order can be reproduced by combining CYM early-time with hydro late-evolution evolutions; however in the calculations of [51]

a small deviation from equilibrium has to be assumed in order to use viscous hydrodynamical equations. Therefore it will be interesting to compute the higher order harmonics combining the CYM initial spectrum with the dynamics embedded in the kinetic equations where the assumption of sudden thermalization can be relaxed.

Finally, we have also computed the invariant gluon distribution functions, f_g , for the fKLN glasma and Glauber initial conditions. We have found that the initial longitudinal expansion strongly affects the evolution of these distributions at early times, causing their lowering of one order of magnitude within 1 fm/c for $p_T \gtrsim 1$ GeV. On the other hand at $p_T \lesssim 0.5$ GeV the longitudinal expansion is compensated by the fast thermalization and even without including $(1+f)$ enhancement factors $\langle f \rangle$ stays larger than unity for a time interval $\Delta\tau \sim 2$ fm/c. this suggested that even in the fast expanding QGP in HIC a transient Bose-Einstein condensation can take place as suggested in [48, 49, 90]. However the effect of Bose statistics should be relevant at $p_T \sim T$, while our effect is related to the initial non-equilibrium and not to the final exact distribution. In order to verify quantitatively how this attractor works in presence of the longitudinal expansion we have to perform simulations with Bose enhancement factors in the collision integral kernel, which is beyond the scope of the present study but that we will perform in the near future.

Acknowledgements. The authors acknowledge enlightening discussions with M. Chernodub, J. Y. Ollitrault and N. Su. M. R. acknowledges Mei Huang for her kind hospitality at Institute of High Energy Physics in Beijing, where part of this work was completed. V. G. and F. S. acknowledge the ERC-StG funding under the QGPDyn grant.

-
- [1] STAR, J. Adams et al., Nucl. Phys. **A757**, 102 (2005); PHENIX, K. Adcox et al., Nucl. Phys. **A757**, 184 (2005).
[2] K. Aamodt et al. [ALICE Collaboration], Phys. Rev. Lett. **105**, 252302 (2010).
[3] B. V. Jacak and B. Muller, *Science* **337**, 310 (2012).
[4] R. J. Fries, V. Greco and P. Sorensen, Ann. Rev. Nucl. Part. Sci. **58** (2008) 177
[5] L. P. Csernai, J. I. Kapusta and L. D. McLerran, Phys. Rev. Lett. **97** (2006) 152303
[6] R. A. Lacey *et al.*, Phys. Rev. Lett. **98**, 092301 (2007).
[7] P. Kovtun, D. T. Son, and A. O. Starinets, Phys. Rev. Lett. **94**, 111601 (2005).
[8] V. P. Konchakovski, E. L. Bratkovskaya, W. Cassing, V. D. Toneev and V. Voronyuk, Phys. Rev. C **85** (2012) 011902
[9] J. Y. Ollitrault, Phys. Rev. D **46**, 229 (1992).
[10] P. Romatschke and U. Romatschke, Phys. Rev. Lett. **99**, 172301 (2007).
[11] H. Song and U.W. Heinz, Phys. Rev. C **78**, 024902 (2008).
[12] L. Cifarelli, L. P. Csernai and H. Stoecker, Europhys. News **43N2** (2012) 29
[13] H. Song, S. A. Bass, U. Heinz, T. Hirano and C. Shen, Phys. Rev. C **83**, 054910 (2011) [Erratum-ibid. C **86**, 059903 (2012)].
[14] B. Schenke, S. Jeon and C. Gale, Phys. Rev. C **82** (2010) 014903
[15] H. Niemi, G. S. Denicol, P. Huovinen, E. Molnar and D. H. Rischke, Phys. Rev. Lett. **106** (2011) 212302
[16] Z. Xu and C. Greiner, Phys. Rev. C **79** (2009) 014904
[17] Z. Xu, C. Greiner and H. Stoecker, Phys. Rev. Lett. **101** (2008) 082302
[18] E. L. Bratkovskaya, W. Cassing, V. P. Konchakovski and O. Linnyk, Nucl. Phys. A **856** (2011) 162
[19] G. Ferini, M. Colonna, M. Di Toro and V. Greco, Phys. Lett. B **670**, 325 (2009)
[20] S. Plumari and V. Greco, AIP Conf. Proc. **1422** (2012) 56
[21] M. Ruggieri, F. Scardina, S. Plumari and V. Greco, Phys. Lett. B **727**, 177 (2013).
[22] L. D. McLerran and R. Venugopalan, Phys. Rev. D **49**, 2233 (1994)

- [23] L. D. McLerran and R. Venugopalan, Phys. Rev. D **49**, 3352 (1994)
- [24] L. D. McLerran and R. Venugopalan, Phys. Rev. D **50**, 2225 (1994).
- [25] F. Gelis, E. Iancu, J. Jalilian-Marian and R. Venugopalan, Ann. Rev. Nucl. Part. Sci. **60**, 463 (2010).
- [26] E. Iancu and R. Venugopalan, In *Hwa, R.C. (ed.) et al.: Quark gluon plasma* 249-3363.
- [27] L. McLerran, arXiv:0812.4989 [hep-ph]; hep-ph/0402137.
- [28] F. Gelis, Int. J. Mod. Phys. A **28**, 1330001 (2013).
- [29] Y. V. Kovchegov, Phys. Rev. D **60** (1999) 034008
- [30] M. Luzum and P. Romatschke, Phys. Rev. C **78** (2008) 034915 [Erratum-ibid. C **79** (2009) 039903]
- [31] B. H. Alver, C. Gombaud, M. Luzum and J. -Y. Ollitrault, Phys. Rev. C **82** (2010) 034913
- [32] A. Adare *et al.* [PHENIX Collaboration], Phys. Rev. Lett. **107**, 252301 (2011).
- [33] M. L. Miller, K. Reygers, S. J. Sanders and P. Steinberg, Ann. Rev. Nucl. Part. Sci. **57**, 205 (2007)
- [34] D. Kharzeev, E. Levin and M. Nardi, Nucl. Phys. A **747**, 609 (2005); D. Kharzeev, E. Levin and L. McLerran, Phys. Lett. B **561**, 93 (2003); D. Kharzeev and M. Nardi, Phys. Lett. B **507**, 121 (2001); D. Kharzeev and E. Levin, Phys. Lett. B **523**, 79 (2001); T. Hirano and Y. Nara, Nucl. Phys. A **743**, 305 (2004).
- [35] T. Hirano, U. W. Heinz, D. Kharzeev, R. Lacey and Y. Nara, Phys. Lett. B **636**, 299 (2006)
- [36] H. -J. Drescher and Y. Nara, Phys. Rev. C **75**, 034905 (2007); Phys. Rev. C **76**, 041903 (2007).
- [37] T. Hirano and Y. Nara, Phys. Rev. C **79**, 064904 (2009)
- [38] J. L. Albacete and C. Marquet, Phys. Rev. Lett. **105**, 162301 (2010); Phys. Lett. B **687**, 174 (2010).
- [39] T. Lappi and R. Venugopalan, Phys. Rev. C **74**, 054905 (2006)
- [40] L. V. Gribov, E. M. Levin and M. G. Ryskin, Phys. Rept. **100**, 1 (1983).
- [41] Y. V. Kovchegov and K. Tuchin, Phys. Rev. D **65**, 074026 (2002)
- [42] J. L. Albacete and A. Dumitru, arXiv:1011.5161 [hep-ph].
- [43] S. Plumari, V. Baran, M. Di Toro, G. Ferini and V. Greco, Phys. Lett. B **689**, 18 (2010).
- [44] S. Plumari, A. Puglisi, M. Colonna, F. Scardina and V. Greco, J. Phys. Conf. Ser. **420**, 012029 (2013).
- [45] S. Plumari, A. Puglisi, F. Scardina and V. Greco, Phys. Rev. C **86** (2012) 054902.
- [46] A. El, Z. Xu and C. Greiner, Nucl. Phys. A **806** (2008) 287.
- [47] O'Hara K M, Hemmer S L, Gehm M E, Granade S R and Thomas J E 2002, *Science* **298** 2179.
- [48] J. -P. Blaizot *et al.*, arXiv:1305.2119 [hep-ph]; J. -P. Blaizot *et al.*, Nucl. Phys. A904-905 **2013**, 829c (2013).
- [49] J. -P. Blaizot, F. Gelis, J. Liao, L. McLerran and R. Venugopalan, Nucl. Phys. A904-905 **2013** (2013) 829c
- [50] H. -J. Drescher, A. Dumitru, A. Hayashigaki and Y. Nara, Phys. Rev. C **74**, 044905 (2006).
- [51] C. Gale, S. Jeon, B. Schenke, P. Tribedy and R. Venugopalan, Phys. Rev. Lett. **110**, 012302 (2013).
- [52] R. Ryblewski and W. Florkowski, Phys. Rev. D **88**, 034028 (2013).
- [53] F. Gelis and T. Epelbaum, arXiv:1307.2214 [hep-ph].
- [54] K. Fukushima, arXiv:1307.1046 [hep-ph].
- [55] J. -P. Blaizot, T. Lappi and Y. Mehtar-Tani, Nucl. Phys. A **846**, 63 (2010).
- [56] T. Lappi, Phys. Lett. B **703**, 325 (2011).
- [57] T. Lappi, Eur. Phys. J. C **71**, 1699 (2011).
- [58] C. Shen, U. W. Heinz, J. -F. Paquet and C. Gale, arXiv:1308.2440 [nucl-th].
- [59] C. Shen, U. W. Heinz, J. -F. Paquet, I. Kozlov and C. Gale, arXiv:1308.2111 [nucl-th].
- [60] H. Song, S. Bass and U. W. Heinz, arXiv:1311.0157 [nucl-th].
- [61] U. Heinz and R. Snellings, Ann. Rev. Nucl. Part. Sci. **63**, 123 (2013).
- [62] J. S. Moreland, Z. Qiu and U. W. Heinz, Nucl. Phys. A904-905 **2013**, 815c (2013).
- [63] J. L. Albacete, A. Dumitru and Y. Nara, J. Phys. Conf. Ser. **316**, 012011 (2011).
- [64] Z. Qiu and U. W. Heinz, Phys. Rev. C **84**, 024911 (2011).
- [65] H. Song, S. A. Bass and U. Heinz, Phys. Rev. C **83**, 054912 (2011) [Erratum-ibid. C **87**, 019902 (2013)].
- [66] A. Monnai and T. Hirano, Phys. Lett. B **703**, 583 (2011).
- [67] T. Hirano, P. Huovinen and Y. Nara, Phys. Rev. C **84**, 011901 (2011).
- [68] H. Song and U. W. Heinz, Phys. Lett. B **658**, 279 (2008).
- [69] J. Adams *et al.* [STAR Collaboration], Phys. Rev. C **72**, 014904 (2005).
- [70] C. Shen and U. Heinz, Phys. Rev. C **83**, 044909 (2011).
- [71] H. Song and U. W. Heinz, Phys. Rev. C **78**, 024902 (2008).
- [72] P. Romatschke, Int. J. Mod. Phys. E **19**, 1 (2010).
- [73] D. A. Teaney, arXiv:0905.2433 [nucl-th].
- [74] P. Huovinen and D. Molnar, Phys. Rev. C **79**, 014906 (2009).
- [75] A. El, Z. Xu and C. Greiner, Phys. Rev. C **81** (2010) 041901
- [76] V. Greco, Anisotropic Flow from a Kinetic Theory Approach, Talk given at INPC 2013, 2-6 June 2013, Florence (Italy).
- [77] C. Greiner, private communication.
- [78] H. Grad, Commun. Pure Appl. Math. **2**, (1949) 331; H. Grad, Commun. Pure Appl. Math. **2**, (1949) 325.
- [79] G. S. Denicol, E. Molnar, H. Niemi and D. H. Rischke, Eur. Phys. J. A, **48** **11** (2012) 170g
- [80] M. Prakash, M. Prakash, R. Venugopalan, and G. Welke, Phys. Rept. **227**, 321 (1993).
- [81] J.-W. Chen, Y.-H. Li, Y.-F. Liu, and E. Nakano, Phys. Rev. **D76**, 114011 (2007), hep-ph/0703230.
- [82] N. Demir and S. A. Bass, Phys.Rev.Lett. **102**, 172302 (2009), 0812.2422.
- [83] P. B. Arnold, G. D Moore and L. G. Yaffe, JHEP **0305**, 051 (2003).
- [84] K. Tsumura and T. Kunihiro, arXiv:1311.7059 [physics.flu-dyn].
- [85] D. Bazow, U. W. Heinz and M. Strickland, arXiv:1311.6720 [nucl-th].
- [86] S. Plumari, A. Puglisi, F. Scardina and V. Greco, J. Phys. Conf. Ser. **446**, 012025 (2013).
- [87] B. Alver *et al.*, Phys. Rev. C **83**, 024913 (2011).
- [88] K. Aamodt *et al.*, Phys. Rev. Lett. **106** (2011) 032301.
- [89] J. Adams *et al.*, Phys. Rev. Lett. **91** (2003) 172302.
- [90] X. -G. Huang and J. Liao, Int. J. Mod. Phys. E **23** (2014) 1430003